

Tidal Deformability of Quark Stars with Repulsive Interactions

M. B. Albino[†], R. Fariello^{†‡} and F. S. Navarra[†]

† Instituto de Física, Universidade de São Paulo

Rua do Matão, 1371, 05508-090, Cidade Universitária, São Paulo, SP, Brazil and

‡ Departamento de Ciências da Computação,

Universidade Estadual de Montes Claros,

Avenida Rui Braga, sn, Vila Mauricéia,

Montes Claros, 39401-089, Minas Gerais, Brazil

Abstract

In an early work, we applied a QCD-based EOS to the study of the stellar structure of self-bound strange stars, obtaining sequences with maximum masses larger than two solar masses and radii ranging from 8 to 12 Km. In this work, we update the previous calculations and compare them with the most recent data, including the very recent determination of the mass and radius of the massive pulsar PSR J0740+6620 performed by the NICER and XMM-Newton Collaborations. Our equation of state is similar to the MIT bag model one, but it includes repulsive interactions, which turn out to be essential to reproduce the accumulated experimental information. We find that our EOS is still compatible with all astrophysical observations but the parameter window is now narrower.

I. INTRODUCTION

The region of the QCD phase diagram with low temperature and high chemical potential is still not well understood. From the theoretical point of view, there are no accurate first principles predictions for the properties of QCD matter at high baryon densities. The numerical lattice simulation techniques that have been successfully applied to the study of the hot quark gluon plasma (QGP) fail in the cold, baryon rich conditions due to the sign problem. In spite of the difficulties, significant progress has been accomplished both in the theoretical description of moderate density nuclear matter [1, 2] and ultrahigh-density matter [3, 4] but no reliable results exist in the crucial regime between approximately one and ten nuclear saturation densities. Several model calculations suggest that there is a low temperature deconfined phase of quarks and gluons, the cold QGP, also called quark matter (QM). This phase might exist in the the core of dense stars, an idea that has been around already for some decades [5, 6]. It is even possible that a whole star, not only its core, be made of quark matter [7]. This possibility was explored in several works [8–12] and will be further explored in this work, which is an update of [10].

An early analysis of the existing observational data presented in [13] concluded that most of the QM EOSs were too soft and therefore unable to support the existence of neutron stars with a quark phase. Since then it was shown in several works that a self-bound star, composed entirely of quark matter, could explain a massive neutron star. In order to obtain a stiff enough quark matter equation of state, several groups introduced repulsive interactions among the quarks, mediated by the exchange of vector particles [10, 14–19], which can be “effective massive gluons” or “effective vector mesons”. Interestingly, most of these developments make use of a mean field approximation for the vector field and arrive at a similar result, which is a quadratic term in the baryon density present both in the pressure and energy density.

From the experimental side, during the last decade we have witnessed remarkable advances in the observation of neutron stars: the discovery of extremely massive neutron stars [20, 21]; qualitative improvements in X-ray radius measurements [22–28]; and the famous LIGO/Virgo detection of gravitational waves (GWs) originating from the NS-NS merger GW170817 [29]. Increasingly stringent constraints have been placed on the EOS of NS matter. An accurate measurement of a compact object using Shapiro delay [30] yielded

$2.14_{-0.09}^{+0.1} M_{\odot}$ for the J0740+6620 pulsar. It has been argued that a handful of compact stars may achieve masses greater than the PSR J0740+6620. The events denoted as GW190814 [31] and GW190425 [32] suggest that the NS mass can be larger than $2.5 M_{\odot}$. Recent data (including a reliable determination of the radius) about the pulsar PSR J0030+0451 were published in Refs. [33–37]. Finally, very recently [38] the NICER and XMM-Newton Collaborations presented a determination of the mass and radius of the massive pulsar PSR J0740+6620.

Differences between candidate EOSs can have a significant effect on the tidal interactions of neutron stars. Recently new constraints appeared on the tidal deformability [39]. It has been realized [40] that the two-solar-mass constraint forces the EOS to be relatively stiff at low densities. At the same time, the constraint on $\Lambda(1.4 M_{\odot})$ sets an upper limit for the stiffness, constraining the EOS band in a complementary direction.

In this paper we will update the study presented in [10] and check whether the EOS introduced in [41] remains a viable option, satisfying the most recent experimental constraints.

This text is organized as follows. In Sec. II we briefly review the EOS for the cold QGP. In Sec. III we introduce the stability conditions and discuss its consequences. In Sec. IV we present the Tolman-Oppenheimer-Volkoff (TOV) equations for stellar structure calculations and their numerical solutions. In Sec. V we discuss the tidal deformability and in Sec. VI we present some comments and conclusions.

II. THE EQUATION OF STATE

Following [10], we consider a quark star consisting of u , d and s quarks with masses $m_u = 5$ MeV, $m_d = 7$ MeV, and $m_s = 100$ MeV. The derivation of the EOS [41] used here starts with the assumption that the gluon field can be decomposed into low (“soft”) and high (“hard”) momentum components. The expectation values of the soft fields were identified with the gluon condensates of dimension two and four, respectively. The former generates a dynamical mass, m_G for the hard gluons, and the latter yields an analogue of the “bag constant” term in the energy density and pressure. Given the large number of quark sources, even in the weak coupling regime, the hard gluon fields are strong, the occupation numbers are large, and therefore these fields can be approximated by classical color fields. The effect of the condensates is to soften the EOS whereas the hard gluons significantly stiffen it, by

increasing both the energy density and pressure. With these approximations it was possible to derive [41] an analytical expression for the EOS, called MFTQCD (Mean Field Theory of QCD). When adapting this equation of state to the stellar medium, we assume, as usual, that quarks and electrons are in chemical equilibrium maintained by the weak processes [42]. Neutrinos are assumed to escape and do not contribute to the pressure and energy density. Moreover, we impose charge neutrality and baryon number conservation. These requirements yield a set of four algebraic equations for Fermi momentum calculation for each quark flavor (u , d and s) and for the electrons (e)

$$\begin{aligned}
k_u^3 + k_d^3 + k_s^3 &= 3\pi^2 \rho_B, \\
2k_u^3 &= k_d^3 + k_s^3 + k_e^3, \\
k_d^2 + m_d^2 &= k_s^2 + m_s^2, \\
\sqrt{k_u^2 + m_u^2} + \sqrt{k_e^2 + m_e^2} &= \sqrt{k_s^2 + m_s^2},
\end{aligned} \tag{1}$$

for a fixed baryon density ρ_B . The energy density is given by [41]

$$\begin{aligned}
\epsilon &= \left(\frac{27g^2}{2m_G^2} \right) \rho_B^2 + \mathcal{B}_{QCD} \\
&+ \sum_{i=u,d,s} 3 \frac{\gamma_Q}{2\pi^2} \left\{ \frac{k_i^3 \sqrt{k_i^2 + m_i^2}}{4} + \frac{m_i^2 k_i \sqrt{k_i^2 + m_i^2}}{8} - \frac{m_i^4}{8} \ln \left[k_i + \sqrt{k_i^2 + m_i^2} \right] + \frac{m_i^4}{16} \ln(m_i^2) \right\} \\
&+ \frac{\gamma_e}{2\pi^2} \left\{ \frac{k_e^3 \sqrt{k_e^2 + m_e^2}}{4} + \frac{m_e^2 k_e \sqrt{k_e^2 + m_e^2}}{8} - \frac{m_e^4}{8} \ln \left[k_e + \sqrt{k_e^2 + m_e^2} \right] + \frac{m_e^4}{16} \ln(m_e^2) \right\}, \tag{2}
\end{aligned}$$

and the pressure is

$$\begin{aligned}
p &= \left(\frac{27g^2}{2m_G^2} \right) \rho_B^2 - \mathcal{B}_{QCD} \\
&+ \sum_{i=u,d,s} \frac{\gamma_Q}{2\pi^2} \left\{ \frac{k_i^3 \sqrt{k_i^2 + m_i^2}}{4} - \frac{3m_i^2 k_i \sqrt{k_i^2 + m_i^2}}{8} + \frac{3m_i^4}{8} \ln \left[k_i + \sqrt{k_i^2 + m_i^2} \right] - \frac{3m_i^4}{16} \ln(m_i^2) \right\} \\
&+ \frac{\gamma_e}{6\pi^2} \left\{ \frac{k_e^3 \sqrt{k_e^2 + m_e^2}}{4} - \frac{3m_e^2 k_e \sqrt{k_e^2 + m_e^2}}{8} + \frac{3m_e^4}{8} \ln \left[k_e + \sqrt{k_e^2 + m_e^2} \right] - \frac{3m_e^4}{16} \ln(m_e^2) \right\}, \tag{3}
\end{aligned}$$

where $m_e = 0.5$ MeV is the electron mass, m_G is the dynamical gluon mass, and g is the coupling constant ($\alpha_s = g^2/4\pi$) in QCD. Our analogue of the bag constant, called here \mathcal{B}_{QCD} , is given by

$$\mathcal{B}_{QCD} = \frac{9}{128} \phi_0^4 = \left\langle \frac{1}{4} F^{a\mu\nu} F_{\mu\nu}^a \right\rangle, \tag{4}$$

where ϕ_0 is an energy scale associated with the energy density of the vacuum and with the gluon condensate [41]. In (2) and (3) the summation over quark colors has already been performed. Throughout this work we employ the natural units $G = 1$, $\hbar = 1$, $c = 1$. Comparing Eqs. (2) and (3) with the equivalent definitions of energy and pressure in the modified bag model with postulated repulsive vector interactions (see Eqs. (14) and (16) of Ref. [43]), we observe a similarity. Both EOSs have a term proportional to ρ_B^2 . In [41] it was derived from QCD whereas in [43] it was postulated.

III. STABILITY CONDITIONS

In this section we discuss the two stability conditions, which have to be satisfied by stable strange quark matter. The first one is that the energy per baryon of the deconfined phase (for $P = 0$ and $T = 0$) is lower than the nonstrange infinite baryonic matter defined in [12, 42]. Following these works we impose that:

$$E_A \equiv \frac{\epsilon}{\rho_B} \leq 934 \text{ MeV}. \quad (5)$$

This condition must hold at the zero pressure point and hence we can, from (2) and (3), numerically derive a relation between the bag constant B_{QCD} and the ratio $\xi = g/m_G$. We solve (3) obtaining $\rho_B = \rho_B(B_{QCD}, \xi)$, which is then inserted into (2). The resulting expression is used to write the condition $\epsilon(B_{QCD}, \xi)/\rho_B(B_{QCD}, \xi) = 934 \text{ MeV}$, which defines one “stability frontier”. This last equation is rewritten as $\xi = \xi(B_{QCD})$, is plotted in Fig. 1 (solid line) and denoted by the 3-flavor line. Points in the (B_{QCD}, ξ) plane located on the right of the solid line are discarded since they do not satisfy (5). The solid line, corresponding to the maximal value of $E_A = 934 \text{ MeV}$, determines the maximum value of B_{QCD} . The minimum value of B_{QCD} is determined by the second stability condition, which requires nonstrange quark matter in the bulk to have an energy per baryon higher than the one of nonstrange infinite baryonic matter. By imposing that

$$E_A \equiv \frac{\epsilon}{\rho_B} \geq 934 \text{ MeV}, \quad (6)$$

for a two flavor quark matter at ground state, we ensure that atomic nuclei do not dissolve into their constituent quarks. The constraint (6) defines the dashed line in the (B_{QCD}, ξ) plane, denoted by the 2-flavor line in Fig. 1. Points located on the left of this line are

excluded because they do not satisfy (6). The region between the two lines in Fig. 1 defines our stability window. Having fixed the \mathcal{B}_{QCD} and ξ parameters, we go back to (2) and (3)

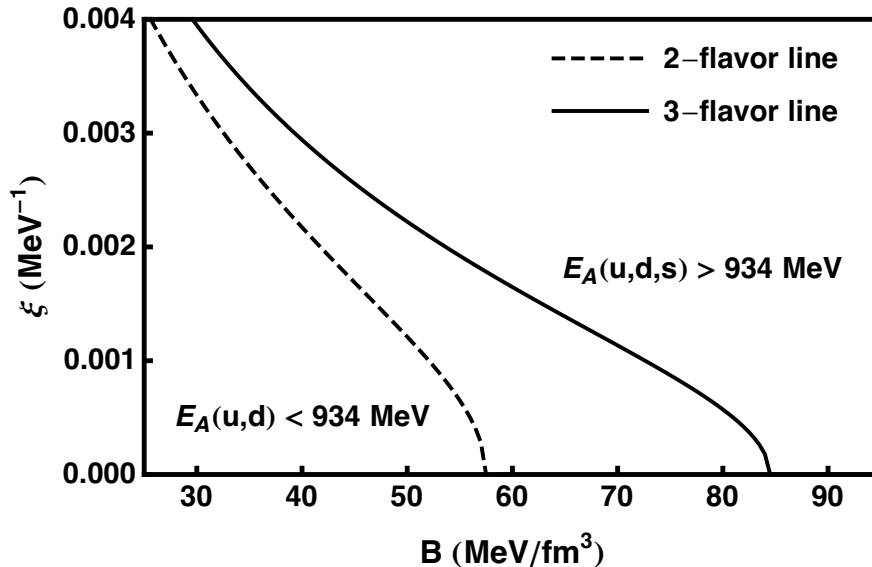


FIG. 1: Values of $\xi = g/m_G$ as a function of \mathcal{B}_{QCD} for different values of the energy per baryon. The two lines define the stability region.

and, obtaining ϵ and p for successive values of ρ_B , we construct the EOS in the form $p = p(\epsilon)$, plotted in Fig. 2a. In the figure, the different lines correspond to the three parameter sets listed in Table I. In this type of plot the slope is the speed of sound, which, due to causality, can not exceed the unity. This limit is shown by the full lines in the figure. In Fig. 2b we show the corresponding values of the speed of sound. As it can be seen, our model yields a much stiffer EOS, with a speed of sound much larger than the conformal value, for which $c_s^2 = 1/3$. The dot-dashed line shows the EOS obtained from a recently updated version of the MIT bag model [44, 45], which reads

$$p(\epsilon) = \frac{(\epsilon - B_{eff})}{3} - \frac{a_2^2}{12\pi^2 a_4} \left[1 + \sqrt{1 + \frac{16\pi^2 a_4}{a_2^2} (\epsilon - B_{eff})} \right], \quad (7)$$

where $B_{eff}^{1/4} = 142.52$ MeV, $a_2^{1/2} = 100$ MeV and $a_4 = 0.535$. As it can be seen, the MFTQCD EOS generates stronger pressure for larger values of the parameter $\xi = g/m_G$. This combination of parameters appears in the first term of (3), which comes from the repulsive interactions [41].

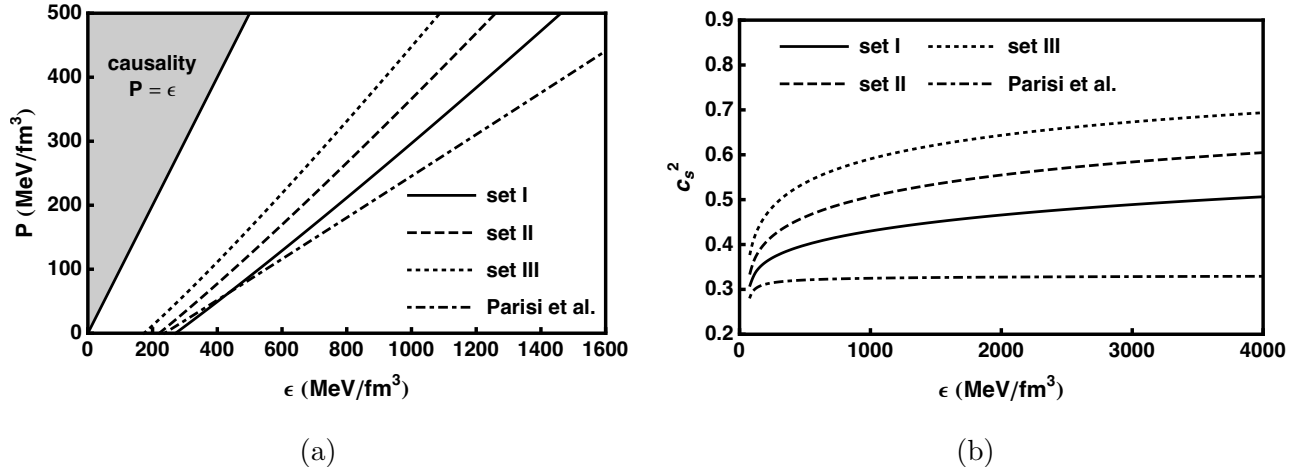


FIG. 2: a) Equation of state obtained with MFTQCD. Set I, II and III correspond to the parameter combinations shown in Table I. For comparison, the dot-dashed line show the MIT Bag Model EOS used by Parisi et al. in Ref. [45]. b) Speed of sound for the same parameter choices.

IV. TOV EQUATION, MASS AND RADIUS

In order to describe the structure of a static, non-rotating compact star, we use the Tolman-Oppenheimer-Volkoff (TOV) equation for the pressure $p(r)$ [46]:

$$\frac{dp}{dr} = -\frac{\epsilon(r)M(r)}{r^2} \left[1 + \frac{p(r)}{\epsilon(r)} \right] \left[1 + \frac{4\pi r^3 p(r)}{M(r)} \right] \times \left[1 - \frac{2M(r)}{r} \right]^{-1}. \quad (8)$$

The enclosed mass $M(r)$ of the compact star is given by the mass continuity equation:

$$\frac{dM(r)}{dr} = 4\pi r^2 \epsilon(r). \quad (9)$$

Equations (8) and (9) express the balance between the gravitational force and the internal pressure acting on a shell of mass $dM(r)$ and thickness dr .

We solve numerically (8) and (9) for $p(r)$ and $M(r)$, to obtain the mass-radius diagram. The pressure and the energy density in (8) and (9) are given by the MFTQCD expressions (3) and (2), respectively. We take the central energy density to be $\epsilon(r=0) = \epsilon_c$ and then we integrate out (8) and (9) from $r=0$ up to $r=R$, where the pressure at the surface is zero: $p(r=R) = 0$. In Fig. 3 we show the mass-radius diagram for several values of \mathcal{B}_{QCD} and ξ respecting the stability condition. In the diagram, the points represent the region favored by the measurements reported in Refs. [33–38]. We can see that, with the parameters chosen in

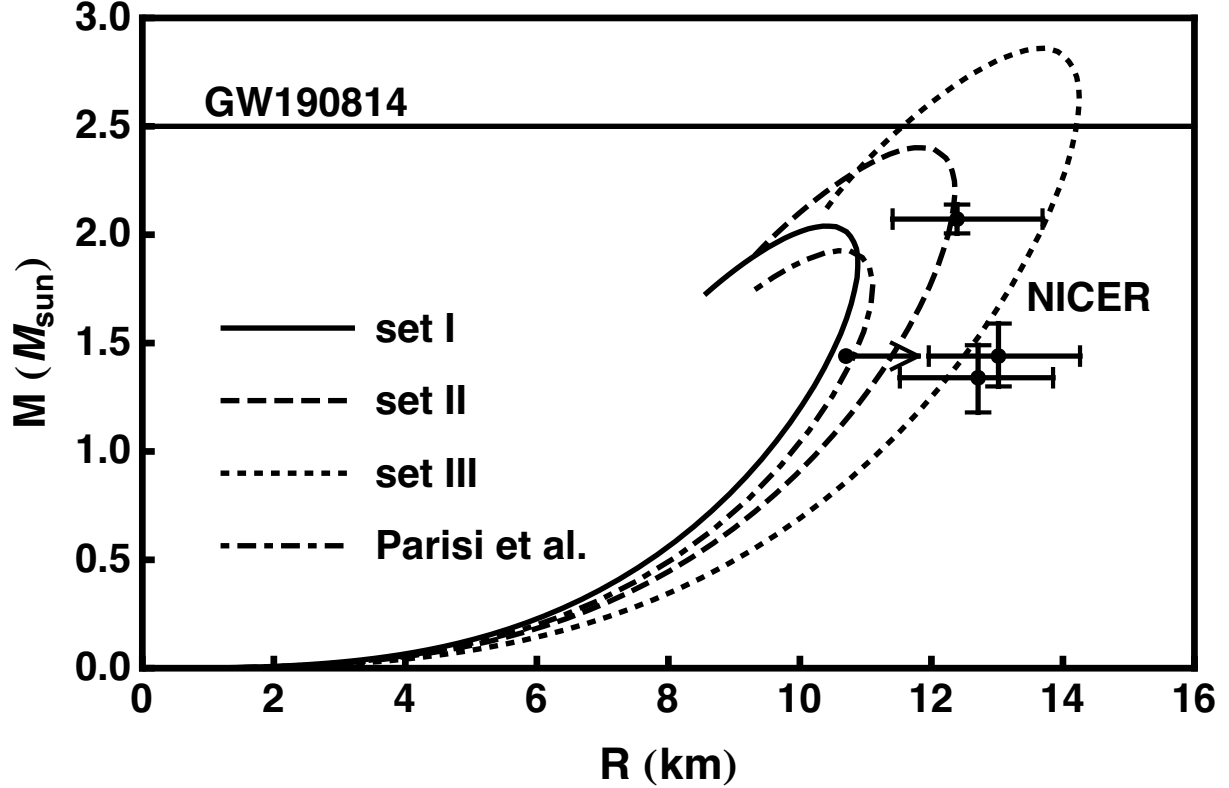


FIG. 3: Mass-radius diagram for combinations of \mathcal{B}_{QCD} and ξ allowed by the stability conditions. Set I, II and III correspond to the parameter combinations shown in Table I. The points represent the region favored by the measurements reported by the NICER and XMM-Newton Collaborations [33–38]. The horizontal line shows the mass of the compact object observed in the event GW190814.

the indicated range, our EOS is able to satisfy all the constraints shown in the mass-radius diagram.

TABLE I: Parameter sets used in the figures.

Set	$\mathcal{B}_{QCD}(MeV/fm^3)$	$\xi(MeV^{-1})$
I	70	0.0011
II	60	0.0016
III	50	0.0022

V. TIDAL DEFORMABILITY

An object that experiences the tidal force of another object will deform. The susceptibility to deform is often measured using dimensionless quantities that are called Love numbers. The Love number is an interesting quantity because it can be used to probe the dense-matter EOS using data from double-neutron-star-merger events. There are various binary systems where two objects orbit around each other. Because these objects lose energy to gravitational waves, their orbits are not stable. Therefore, they will inevitably approach each other until they finally merge. Around the collision point, the generated gravitational-wave signal is strong enough to be detected by terrestrial instruments.

The tidal deformability parameter is given by [47–49]

$$\Lambda = \frac{2}{3}k_2C^{-5}, \quad (10)$$

where $C \equiv M/R$ is the compactness of the star and k_2 is the tidal Love number, which is given by [47–49]

$$\begin{aligned} k_2 = & \frac{8C^5}{5} (1 - 2C)^2 [2 + 2C(y - 1) - y] \{2C [6 - 3y + 3C(5y - 8)] \\ & + 4C^3 [13 - 11y + C(3y - 2) + 2C^2(1 + y)] \\ & + 3(1 - 2C)^2 [2 - y + 2C(y - 1)] \ln(1 - 2C)\}^{-1}, \end{aligned} \quad (11)$$

where

$$y = \frac{R\beta(R)}{H(R)} - \frac{4\pi R^3\epsilon_{sup}}{M}, \quad \beta(r) = \frac{dH(r)}{dr}. \quad (12)$$

In the above equation, the second term is a correction due to the fact that in our model the energy density at the surface of the star, $\epsilon_{sup} \equiv \epsilon(P = 0)$ is not zero [48]. The functions H and β can be obtained by solving the following system of differential equations:

$$\begin{aligned} H'(r) &= \beta(r), \quad (13) \\ \frac{d\beta}{dr} &= 2 \left(1 - \frac{2M(r)}{r}\right)^{-1} H(r) \left\{ -2\pi \left[5\epsilon(r) + 9P(r) + \frac{\epsilon(r) + P(r)}{dP/d\epsilon} \right] \right. \\ & \quad \left. + \frac{3}{r^2} + 2 \left(1 - \frac{2M(r)}{r}\right)^{-1} \left(\frac{M(r)}{r^2} + 4\pi r P(r) \right)^2 \right\} \\ & \quad + \frac{2\beta(r)}{r} \left(1 - \frac{2M(r)}{r}\right)^{-1} \left[-1 + \frac{M(r)}{r} + 2\pi r^2 (\epsilon(r) - P(r)) \right]. \end{aligned} \quad (14)$$

The Love number k_2 measures how easily the bulk of the matter in a star is deformed. The Love number also encodes information about the star's degree of central condensation. Stars

that are more centrally condensed will have a smaller response to a tidal field, resulting in a smaller Love number. The Love number decreases with increasing compactness, and from Eq. (11) it can be seen that k_2 vanishes at the compactness of a black hole ($M/R = 0.5$) regardless of the EOS dependent quantity y . The tidal Love numbers of strange quark matter stars are qualitatively different from those of hadronic matter stars [48, 50, 51]. The latter decrease strongly for small values of the compactness.

In Fig. 4a we show the Love number k_2 as a function of the compactness C . We expect that a very compact star for any EoS is harder to deform than a less compact one. This is what we see in the figures. It is interesting to observe that the same variation of \mathcal{B}_{QCD} and ξ which produces visible effects in the equation of state and in the mass-radius diagram does not lead to appreciable differences in the k_2 - C plot. The curves shown in Fig. 4a are practically identical to the curves in the analogous plots shown in Refs. [48], [50] and [51], which were obtained with strange quark matter equations of state. This suggests that a wide variety of quark matter EOSs lead to the same values of k_2 . We also note that our curves are close to the one obtained with the ultrarelativistic EOS with the speed of sound $c_s^2 = 1/3$ [51]. For completeness, in Fig. 4b we show the Love number k_2 as a function of the variable y .

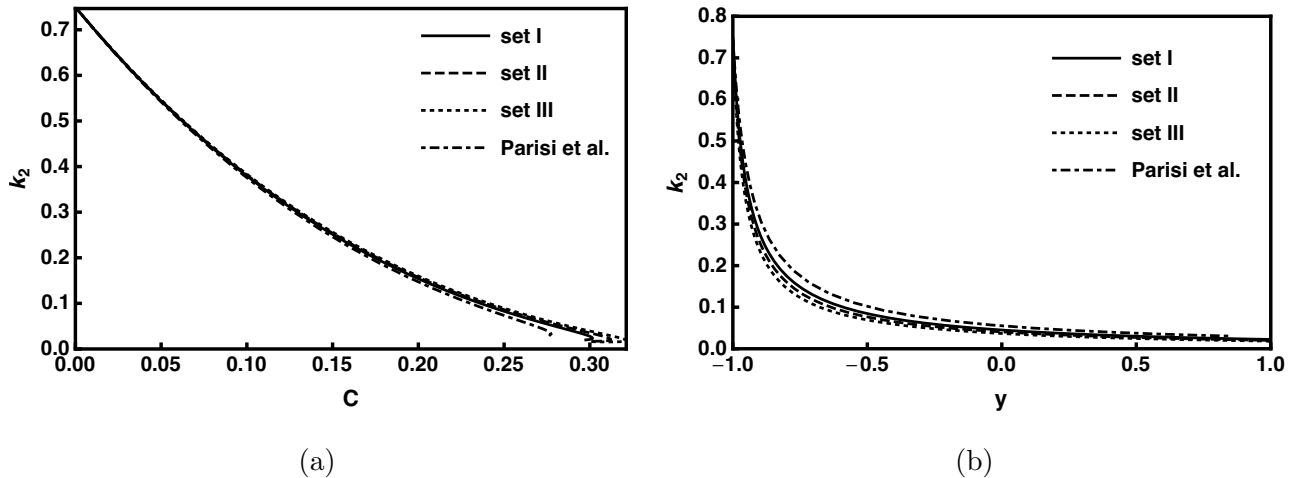


FIG. 4: a) Tidal Love number k_2 as a function of the compactness. b) k_2 as a function of y . The different lines correspond to the three parameter sets listed in Table I.

As pointed out in [48], in contrast to the Love number, the tidal deformability has a wide range of values, spanning roughly an order of magnitude over the observed mass range of neutron stars in binary systems. The updated version of the tidal deformability estimate for

a $1.4 M_{\odot}$ neutron star based on the gravitational-wave event GW170817 [39] implies that

$$70 < \Lambda_{1.4} < 580. \quad (15)$$

In Fig. 5 we show our results for Λ as a function of the star mass M . As it can be seen, the constraint (15) can be satisfied. We note, however, the visible tension between this constraint and those shown in the mass-radius plot. The larger values of the radius required to fit the NICER points seem to be somewhat difficult to reconcile with the Λ values required by the GW170817 estimates. Other calculations performed with quark matter stars [44, 52–55] or hybrid stars [19, 56–60] arrive at similar results. On the other hand, calculations of the tidal deformability with purely hadronic equations of states [61–63] seem to reproduce the experimental data more easily.

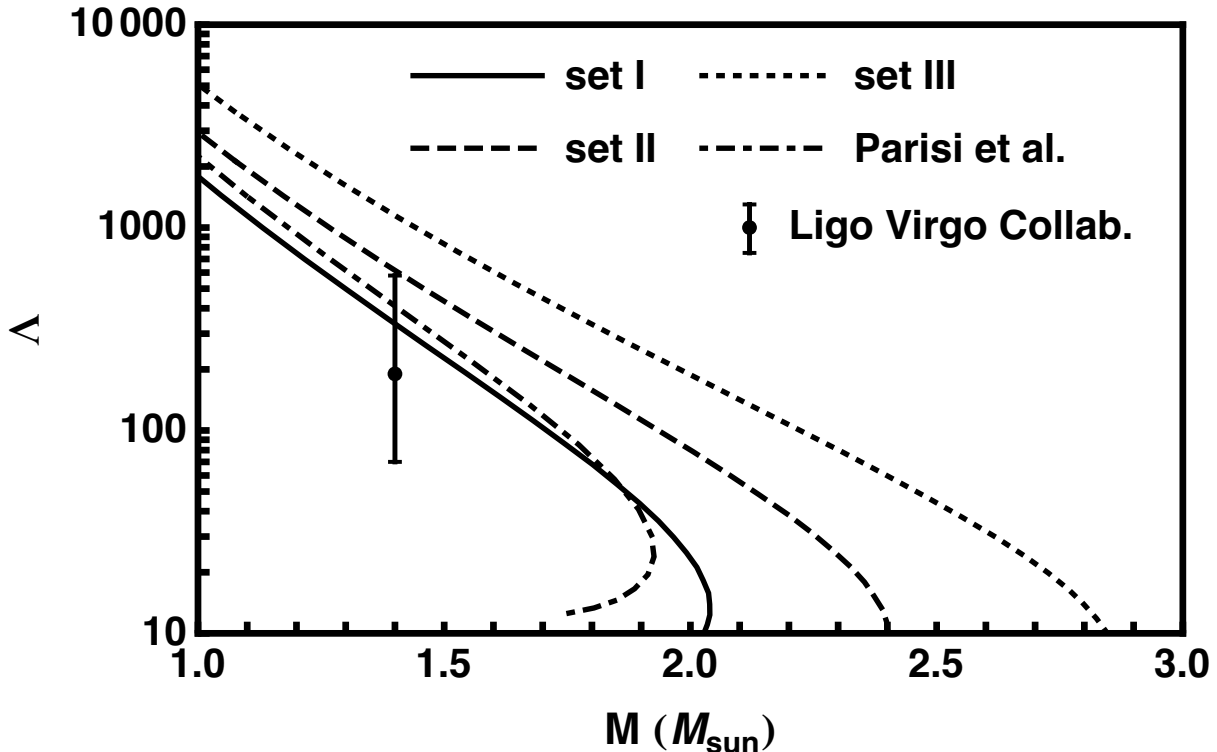


FIG. 5: The tidal deformability parameter Λ as a function of the star mass. The different lines correspond to the three parameter sets listed in Table I. The vertical bar is the empirical tidal deformability at $M = 1.4M_{\odot}$ inferred from the Bayesian analysis of the GW170817 data at the 90% confidence level [39].

VI. CONCLUSION

In [41] a new equation of state for cold quark matter was presented. It was soon applied to the study of neutron stars, treated as self-bound strange quark stars. In this paper, almost ten years later, we have updated the calculations published in [10] and checked whether that EOS can still account for the most recent astrophysical data. We find that MFTQCD is still a viable option. However, we observe that the parameter window is closing. A confirmation of the existing data and the reduction of the error bars in the tidal deformability and in the NICER neutron star radii data will be crucial to rule out strange quark star models and reduce the freedom in the choice of the equation of state.

Acknowledgments

We are deeply grateful to J. Horvath and to G. Lugones for fruitful discussions. This work was partially financed by the Brazilian funding agencies CAPES and CNPq.

-
- [1] M. Oertel, M. Hempel, T. Klöhn and S. Typel, *Rev. Mod. Phys.* **89**, 015007 (2017).
 - [2] I. Tews, T. Krüger, K. Hebeler and A. Schwenk, *Phys. Rev. Lett.* **110**, 032504 (2013).
 - [3] T. Gorda, A. Kurkela, R. Paatelainen, S. Säppi and A. Vuorinen, arXiv:2103.07427 [hep-ph].
 - [4] E. Annala, T. Gorda, A. Kurkela, J. Nättilä and A. Vuorinen, *Nature Phys.* **16**, 907 (2020).
 - [5] D. Ivanenko and D. F. Kurdgelaidze, *Astrophysics J.* **1**, 251 (1965); D. Ivanenko and D. F. Kurdgelaidze, *Lett. Nuovo Cimento* **2**, 13 (1969); N. Itoh, *Prog. Theor. Phys.* **44**, 291 (1970).
 - [6] M. Alford, D. Blaschke, A. Drago, T. Klahn, G. Pagliara, and J. Schaffner-Bielich, *Nature* **445**, E7 (2007).
 - [7] E. Witten, *Phys. Rev. D* **30**, 272 (1984).
 - [8] F. Weber, *Prog. Part. and Nucl. Phys.* **54**, 193 (2005); R. X. Xu, S. I. Bastrukov, F. Weber, J. W. Yu, and I. V. Molodtsova, *Phys. Rev. D* **85**, 023008 (2012); A. Drago, A. Lavagno, and I. Parenti, *Astrophys. J.* **659**, 1519 (2007); J. W. Yu and R. X. Xu, *Mon. Not. R. Astron. Soc.* **414**, 489 (2011); A. Drago, A. Lavagno, and G. Pagliara, *Phys. Rev. D* **89**, 043014 (2014); A. Drago and G. Pagliara, *Phys. Rev. C* **92**, 045801 (2015); A. Drago, A. Lavagno, G. Pagliara, and D. Pigato, *Eur. Phys. J. A* **52**, 40 (2016); A. Drago and G. Pagliara, *Eur. Phys. J. A* **52**,

- 41 (2016); G. Panotopoulos and I. Lopes, *Phys. Rev. D* **96**, 083013 (2017); G. Wiktorowicz, A. Drago, G. Pagliara, and S. B. Popov, *Astrophys. J.* **846**, 163 (2017); J. Bora and U. D. Goswami, *Mon. Not. Roy. Astron. Soc.* **502**, 1557 (2021).
- [9] J. E. Horvath and P. H. R. S. Moraes, *Int. J. Mod. Phys. D* **30**, 2150016 (2021).
- [10] B. Franzon, D. A. Fogaca, F. S. Navarra and J. E. Horvath, *Phys. Rev. D* **86**, 065031 (2012).
- [11] M.G.B. de Avellar, J. E. Horvath, and L. Paulucci, *Phys. Rev. D* **84**, 043004 (2011).
- [12] S. Weissenborn, I. Sagert, G. Pagliara, M. Hempel, and J. Schaffner - Bielich, *Astrophysics J.* **740**, L14 (2011).
- [13] F. Özel, *Nature* **441**, 1115 (2006).
- [14] M. Cierniak, T. Klähn, T. Fischer and N. U. Bastian, *Universe* **4**, 30 (2018); T. Klähn and T. Fischer, *Astrophys. J.* **810**, 134 (2015).
- [15] Y. Song, G. Baym, T. Hatsuda and T. Kojo, *Phys. Rev. D* **100**, 034018 (2019).
- [16] L. L. Lopes, C. Biesdorf, K. D. Marquez and D. P. Menezes, *Phys. Scripta* **96**, 065302 (2021).
L. L. Lopes, C. Biesdorf and D. P. Menezes, arXiv:2005.13136 [hep-ph].
- [17] K. Otto, M. Oertel and B. J. Schaefer, *Eur. Phys. J. ST* **229**, 3629 (2020).
- [18] R. D. Pisarski, *Phys. Rev. D* **103**, L071504 (2021).
- [19] L. Q. Su, Y. Yan, C. M. Li, Y. F. Huang and H. Zong, *Phys. Rev. D* **103**, 094037 (2021).
- [20] J. Antoniadis et al., *Science* **340**, 6131 (2013).
- [21] P. B. Demorest, T. Pennucci, S. M. Ransom, M. S. E. Roberts, and J. W. T. Hessels, *Nature* **467**, 1081 (2010).
- [22] S. Guillot, M. Servillat, N. A. Webb and R. E. Rutledge, *Astrophys. J.* **772**, 7 (2013).
- [23] F. Özel, D. Psaltis, T. Guver, G. Baym, C. Heinke and S. Guillot, *Astrophys. J.* **820**, 28 (2016).
- [24] F. Özel and P. Freire, *Ann. Rev. Astron. Astrophys.* **54**, 401 (2016).
- [25] A. W. Steiner, C. O. Heinke, S. Bogdanov, C. Li, W. C. G. Ho, A. Bahramian and S. Han, *Mon. Not. Roy. Astron. Soc.* **476**, 421 (2018).
- [26] J. Nättilä, A. W. Steiner, J. J. E. Kajava, V. F. Suleimanov and J. Poutanen, *Astron. Astrophys.* **591**, A25 (2016).
- [27] J. Nättilä, M. C. Miller, A. W. Steiner, J. J. E. Kajava, V. F. Suleimanov and J. Poutanen, *Astron. Astrophys.* **608**, A31 (2017).
- [28] S. Bogdanov, C. O. Heinke, F. Özel and T. Güver, *Astrophys. J.* **831**, 184 (2016).

- [29] B. P. Abbott et al. [LIGO Scientific and Virgo Collaborations], Phys. Rev. Lett. **119**, 161101 (2017).
- [30] H. Cromartie et. al. Nature Astronomy **4**, 72 (2020).
- [31] R. Abbott et al. LIGO and Virgo Scientific Collaborations, Astrophys. J. Lett. **896**, L44 (2020).
- [32] B. P. Abbott et al. LIGO Scientific and Virgo Collaborations, Astrophys. J. Lett. **892**, L3 (2020).
- [33] M.C. Miller et al., Astrophys. J. Lett. **887**, L24 (2019).
- [34] T. E. Riley, A. L. Watts, S. Bogdanov, P. S. Ray, R. M. Ludlam, S. Guillot et al., Astrophys. J. Lett. **887**, L21 (2019).
- [35] S. Bogdanov, S. Guillot, P. S. Ray, M. T. Wolff, D. Chakrabarty, W. C. G. Ho et al., Astrophys. J. Lett. **887**, L25 (2019).
- [36] Raaijmakers, G. et al., Astrophys. J. Lett. **887**, L22 (2019).
- [37] C.D. Capano et al., Nature Astron. **4**, 625 (2020).
- [38] T. E. Riley *et al.*, arXiv:2105.06980 [astro-ph.HE].
- [39] R. Abbott et al. LIGO and Virgo Scientific Collaborations, Phys. Rev. Lett. **121**, 161101 (2018).
- [40] Annala, E., Gorda, T., Kurkela, A. and Vuorinen, A., Phys. Rev. Lett. **120**, 172703 (2018).
- [41] D. A. Fogaça, F.S. Navarra, Phys. Lett. B **700**, 236 (2011).
- [42] E. Farhi, R.L. Jaffe, Phys. Rev. D **30**, 2379 (1984).
- [43] M. Cierniak and D. Blaschke, Eur. Phys. J. ST **229**, 3663 (2020).
- [44] E. P. Zhou, X. Zhou and A. Li, Phys. Rev. D **97**, 083015 (2018).
- [45] A. Parisi, C. V. Flores, C. H. Lenzi, C. S. Chen and G. Lugones, arXiv:2009.14274.
- [46] N. Glendenning, *Compact stars*, (Springer, New York, 2000).
- [47] T. Hinderer, arXiv: 0711.2420; E. E. Flanagan and T. Hinderer, Phys. Rev. D **77**, 021502 (2008); T. Hinderer, Astrophys. J. **677**, 1216 (2008).
- [48] T. Hinderer, B. D. Lackey, R. N. Lang, J. S. Read, Phys. Rev. D **81**, 123016 (2010).
- [49] A. Sabatucci *Tidal deformation of neutron stars*, Thesis, La Sapienza – University of Rome (2018).
- [50] S. Postnikov, M. Prakash and J. M. Lattimer, Phys. Rev. D **82**, 024016 (2010).
- [51] A. Zacchi, arXiv:2007.00423.

- [52] O. Lourenço, C. H. Lenzi, M. Dutra, E. J. Ferrer, V. de la Incera, L. Paulucci and J. E. Horvath, arXiv:2104.07825.
- [53] Q. Wang, C. Shi and H. S. Zong, Phys. Rev. D **100**, 123003 (2019); Erratum: [Phys. Rev. D **100**, 129903 (2019)].
- [54] C. Zhang and R. B. Mann, Phys. Rev. D **103**, 063018 (2021).
- [55] C. M. Li, S. Y. Zuo, Y. Yan, Y. P. Zhao, F. Wang, Y. F. Huang and H. S. Zong, Phys. Rev. D **101**, 063023 (2020).
- [56] M. Ferreira, R. Câmara Pereira and C. Providência, Phys. Rev. D **102**, 083030 (2020).
- [57] M. Ju, X. Wu, F. Ji, J. Hu and H. Shen, Phys. Rev. C **103**, 025809 (2021).
- [58] T. F. Motta, A. M. Kalaitzis, S. Antic, P. A. M. Guichon, J. R. Stone and A. W. Thomas, Astrophys. J. **878**, 159 (2019).
- [59] S. Khanmohamadi, H. R. Moshfegh and S. Atashbar Tehrani, Phys. Rev. D **101**, 123001 (2020).
- [60] S. Han and A. W. Steiner, Phys. Rev. D **99**, 083014 (2019).
- [61] T. Zhao and J. M. Lattimer, Phys. Rev. D **98**, 063020 (2018).
- [62] N. H. Tan, D. T. Khoa and D. T. Loan, Eur. Phys. J. A **57**, 153 (2021).
- [63] C. Drischler, S. Han, J. M. Lattimer, M. Prakash, S. Reddy and T. Zhao, Phys. Rev. C **103**, 045808 (2021).